Diameter Control of Single Wall Carbon Nanotubes Synthesized using Chemical Vapor Deposition

Soumyendu Roy,[a,1]* Reeti Bajpai,[a,2] Navneet Soin,[b] Susanta Sinha Roy,[c] James A. McLaughlin,[b] D. S. Misra [a,]

[a] Department of Physics, Indian Institute of Technology Bombay, Mumbai 400076, India

[b] Nanotechnology and Integrated Bioengineering Centre, University of Ulster at Jordanstown, Newtownabbey BT37 0QB, Northern Ireland, United Kingdom

[c] Department of Physics, School of Natural Sciences, Shiv Nadar University, Chithera, Uttar Pradesh, 203207, India.

* Corresponding author. Email: anoyonline@gmail.com, Phone: +972-36407937, +972-525853865

Keywords: Carbon Nanotube, Single Wall Carbon Nanotube, Chemical Vapor Deposition, Chirality, Controlled Synthesis, Raman Spectroscopy

[1] Present address: School of Electrical Engineering and Tel-Aviv University Center for Nanoscience and Nanotechnology, Tel-Aviv University, Tel-Aviv 6997801, Israel

[2] Present address: Department of Materials and Interfaces, Weizmann Institute of Science, Rehovot 76100, Israel

Abstract

Lack of control on the chirality or diameter of single-wall carbon nanotubes (SWCNTs) during synthesis is a major impediment in the path of their widespread commercialization. We demonstrate that the humble technique of catalytic chemical vapor deposition of methane, without any sophisticated catalyst preparation, can provide significant control on the diameter of the synthesized SWCNTs. The catalyst used is a solid solution of the bimetals Fe-Mo or Co-Mo in MgO. The radial breathing modes (RBMs) in the Raman spectra of SWCNTs were used to find out the diameters. Kataura plot along with RBMs was used to study the chirality of the tubes. High concentration of the catalysts (Co:Mo:MgO = 1:0.5:15 and Fe:Mo:MgO = 1:0.5:30) resulted in high yields. However, most of these carbonaceous materials were impurities. Reducing the concentration not only improved the purity and crystallinity (I_D/I_G ratio ~ 0.1), but most importantly reduced the diameter spread of the SWCNTs. Majority of the SWCNTs grown using the low concentration catalysts (Co:Mo:MgO = 1:0.5:300 and Fe:Mo:MgO = 1:0.5:200) were estimated to have diameters lying between 1.13 and 1.65 nm. This narrowing of diameter spread happened for both Fe and Co catalyst systems and depended only on the concentration of the catalyst.

1. Introduction

Chirality of a single wall carbon nanotube (SWCNT) depends upon its diameter and orientation of the graphene sheet, which when rolled up would produce the tube under consideration. Most physical properties of a SWCNT depend on its chirality. Current synthesis techniques produce tubes with a wide range of diameters. However, in most applications one would prefer tubes with a narrow diameter distribution in order to get controllable and predictable outcomes from the experiments or devices. An ensemble of SWCNTs with random diameter distribution will in general have one third metallic and two third semiconducting tubes. But there are several

applications that require the tubes to be either semiconducting (e.g. field effect transistors) or metallic (e.g. interconnects in integrated circuits). Widespread applications of SWCNTs have been limited due to the unavailability of structurally homogeneous tubes [1]. Some attempts have been made to selectively grow SWCNTs with a controlled diameter and/or chirality [2-9]. Generally these are cumbersome and have limited success or applicability. However these are important steps towards achieving chiral-selective growth in the future. To circumvent the problem of controlled synthesis many have focused on techniques aimed at sorting nanotubes according to diameter or selectively removing nanotubes of one type while preserving the other. These involve methods like density gradient based centrifugation [10], physicochemical modification [11], selective elimination by electrical breakdown [12], gas-phase plasma etching [13], microwave irradiation [14], *etc.* [1,15]. These methods too have several disadvantages like low yield, damage to the crystallinity of nanotubes, requirement of further purification steps to remove the materials added, low repeatability, etc. Moreover it is always preferable and economical to have more control at the growth stage itself.

Chemical vapor deposition (CVD) is by far the most popular commercial and laboratory method to synthesize carbon nanotubes (CNTs). It has several advantages like ease of scaling up, low impurity levels, high yield, and better growth control [16]. It involves the catalytic decomposition of hydrocarbons or carbon monoxide on nanoparticles of transition metals or their oxides (Fe, Co, Ni) [17-23]. In this article we demonstrate significant control on the diameter of SWCNTs synthesized using this ubiquitous technique and a simple catalyst preparation method. One of the key aspects of SWCNT synthesis is to tailor the starting material so that the catalyst particles retain a small size. Thus a supporting material is generally added to the catalyst to control the particle size. The choice of the supporting material has been found to influence the dispersion of the transition metal particles and hence the CNT productivity. Improvement in the quality and quantity of the grown SWCNTs is possible by the use of catalyst promoters like Mo [18,20,24]. In our experiments we have used oxides of Fe and Co as catalyst and Mo as the promoter; all finely dispersed in a matrix of MgO. The catalyst was prepared by the combustion method [17,19,25]. Methane and hydrogen are used as the precursor gases. We have used these nanotubes to successfully prepare several kinds of devices [26-28]. Low frequency resonance Raman scattering spectra or the radial breathing modes (RBMs) and the Kataura plot were used

to investigate the structural property of the SWCNTs. By adjusting the concentration of the active material (Fe or Co) in the catalyst we were able to restrict the diameter spread of the tubes to a certain extent and also to optimize the crystallinity and purity of SWCNTs. The strong dependence of the diameter spread on the concentration of catalyst suggests that the concentration controls the size of the catalyst particles formed during the CVD process. The results are promising and further studies can lead to more control on chirality.

2. Experiments and Methods

2.1 *Catalyst preparation:*

MgO supported Fe-Mo (or Co-Mo) bimetallic catalyst was prepared by mixing ferric nitrate nonahydrate (or cobalt(II) acetate tetrahydrate), ammonium heptamolybdate tetrahydrate, magnesium nitrate hexahydrate and citric acid ($C_6H_8O_7$) in appropriate ratios. The catalyst mixture was ground and mixed in a mortar for 1.5 hrs so as to obtain a fine, uniform powder. The mixture was taken in a quartz boat and heated in an open furnace maintained at a temperature of about 620^0 C for 10 minutes. The mixture was cooled and ground again. The resultant powder is a solid solution of Fe and Mo (or Co and Mo) oxides in MgO grains. The X-ray diffraction pattern has been shown in the supporting information (figure S1).

2.2 *SWCNT synthesis:*

A small amount of the catalyst (about 0.8 g) was spread out in a quartz boat and transferred to a furnace. H_2 gas was used to generate an inert atmosphere. Growth of SWCNTs was carried out at a temperature of 960-970^0 C, with H_2 and CH_4 flow rates of 100 and 22 sccm, respectively. CH_4 flow was maintained for 30 minutes. At high temperature the dopants (Fe, Co and Mo) come out of the MgO structure and create nanoparticles. MgO matrix prevents these nanoparticles from agglomerating amongst themselves. At high temperature hydrocarbon breaks releasing carbon atoms which dissolve into the catalyst nanoparticles that are in a molten state. When the nanoparticles get saturated they start precipitating the carbon atoms.

2.3 *Characterization of SWCNTs:*

The microscopic observations of the SWCNTs were carried out in a high resolution transmission electron microscope (TEM, model: JEOL, JEM 2100F). Horiba Jobin Yvon HR 800 confocal micro-Raman spectrometer equipped with an Argon ion laser of wavelength 514.5 nm (2.41 eV) was used to record the Raman spectra. Typical resolution was 0.5cm^{-1} and the spot size was around 1 μm. Raman spectra were also acquired using ISA LabRam system equipped with a 632.8 nm (1.96 eV) He–Ne laser with a spot size of about 2–3 μm, yielding a spectral resolution of better than 2 cm^{-1}. The third spectrometer used was an Avalon Raman Station-CT system with a 785 nm (1.58 eV) laser and a spectral resolution better than 4 cm^{-1}. The scattered signals were recorded in back scattering geometry and at room temperature for all the three cases. To minimize sample heating, laser powers below 5 mW was used

2.4 *Analysis of RBM spectra:*

Resonance Raman spectroscopy is the most trusted technique for structural analysis of SWCNTs. RBM frequency shifts in the Raman spectra of the SWCNTs were analyzed in order to identify their diameters and chiralities. The three different laser energies used cover almost the entire diameter range of SWCNTs up to 3 nm. Similar techniques have been used by several other groups [29-35]. From the RBM frequencies (ω in cm^{-1}) the diameters (d in nm) of the SWCNTs can be calculated using the relation $\omega = \frac{234}{d} + 10$ [33,34]. The RBM spectra were fitted with Lorentzian peaks having full width at half maxima (FWHM) of 16 cm^{-1}. Similar values have been reported by others [32,33,36]. For consistency the width was kept the same for all the samples and across all the laser energies. In general there is some variation among the spectra taken at different spots of the same sample. Hence the spectra obtained at 6-9 different spots were normalized and an average of these was used for fitting. In some cases a small linear baseline correction was required before averaging.

2.5 *Kataura plot:*

The electronic transitions in CNT occur between the two Van Hove singularities that are on the opposite sides of the Fermi level and are mirror images of each other. The energy differences

(denoted by E_{ii}) can be calculated for SWCNTs of all possible chiralities (n,m) and plotted against the corresponding diameters. The resultant is known as the Kataura plot, after its proponent [29,33,37]. Using tight binding approximation for nearest neighbor interactions the dispersion relation for energy (E) of an electron at a point (k_x,k_y) of the Brillouin zone is given by $E(k_x, k_y) = \pm\gamma_0\sqrt{1 + 4\cos\left(\frac{\sqrt{3}k_x a}{2}\right)\cos\left(\frac{k_y a}{2}\right) + 4\cos^2\left(\frac{k_y a}{2}\right)}$, where γ_0 is the nearest neighbour carbon-carbon interaction energy and (a) is the lattice constant (0.246 nm). The overlap integral (s) has been neglected here. The E_{ii} values for semiconducting (S_{ii}) and metallic (M_{ii}) tubes turns out to be $S_{ii} = \frac{2i\gamma_0\pi}{\sqrt{3(n^2+nm+m^2)}}$ and $M_{ii} = \frac{6i\gamma_0\pi}{\sqrt{3(n^2+nm+m^2)}}$, where ($n$,$m$) is the chiral index of the nanotube. A value of 2.9 eV has been used for the interaction energy γ_0 in this article [38-40].

Raman spectrum of SWCNTs is a resonance effect originating from those tubes that have an E_{ii} ~ the laser energy. From the RBM frequencies we can figure out the diameters and using the additional information of the transition energy we can find out the most probable chiralities of the nanotubes from the Kataura plot (the process is illustrated in the supporting information, figure S2). The resonance windows for energy (ΔE) and diameter (Δd) have been kept 0.2 eV and 0.02 nm, respectively. Similar values have been suggested in earlier studies [34,36]. This choice of resonance window imparted a self-consistency to the whole analysis, so that there was at least one tube that matched all the 69 RBM peaks observed in the Raman spectra of all the different samples. The choice of Δd also restricted the maximum number of chirality matches to three. It is also of the same order as the maximum difference between the diameter values predicted by different RBM versus diameter relations reported in literature (these are given in table S1 and plotted in figure S3 of the supporting information). Remarkably a common set of tubes, with some exceptions, could fit the RBM spectra of all the different samples.

It must also be noted that the analysis technique used here is an approximate method. Several finer corrections in the dispersion relation have been proposed like the effect of substrate and environment, trigonal warping, excitonic effects, bundling of SWCNTs, taking into account the interactions between more neighbors in tight binding calculations, *etc*. Other problems with this technique include the empirical nature of the diameter versus RBM frequency relation and the

general inability of resonance Raman scattering to resolve tubes with very similar diameters [36,41,42].

3. Results and Discussions

The different compositions of the catalysts used have been enumerated in table 1. It should be noted that the same acronyms have been used to refer to both the catalysts and the corresponding SWCNT samples obtained from them. Since Mo promotes the activity of the main catalyst i.e. Fe or Co, its concentration w.r.t. the latter has been kept fixed.

Table 1: Different compositions of the catalysts

SWCNT sample	Co:Mo:MgO (by weight)	SWCNT sample	Fe:Mo:MgO (by weight)
Co1	1:0.5:15	Fe1	1:0.5:30
Co4	1:0.5:90	Fe4	1:0.5:90
Co6	1:0.5:300	Fe5	1:0.5:200

Concentrations lower than Co6 or Fe5 did not produce any observable amounts of SWCNTs. Concentrations higher than the maximum ones shown here lead to the production of a large quantity of impurities as discussed later. Other intermediate concentrations were also studied (but these are not shown here). The following figures (from 1 to 3) and tables (from 2 to 4) depict the fitting of the RBM spectra of the different samples and the estimated diameters and chiralities of the nanotubes.

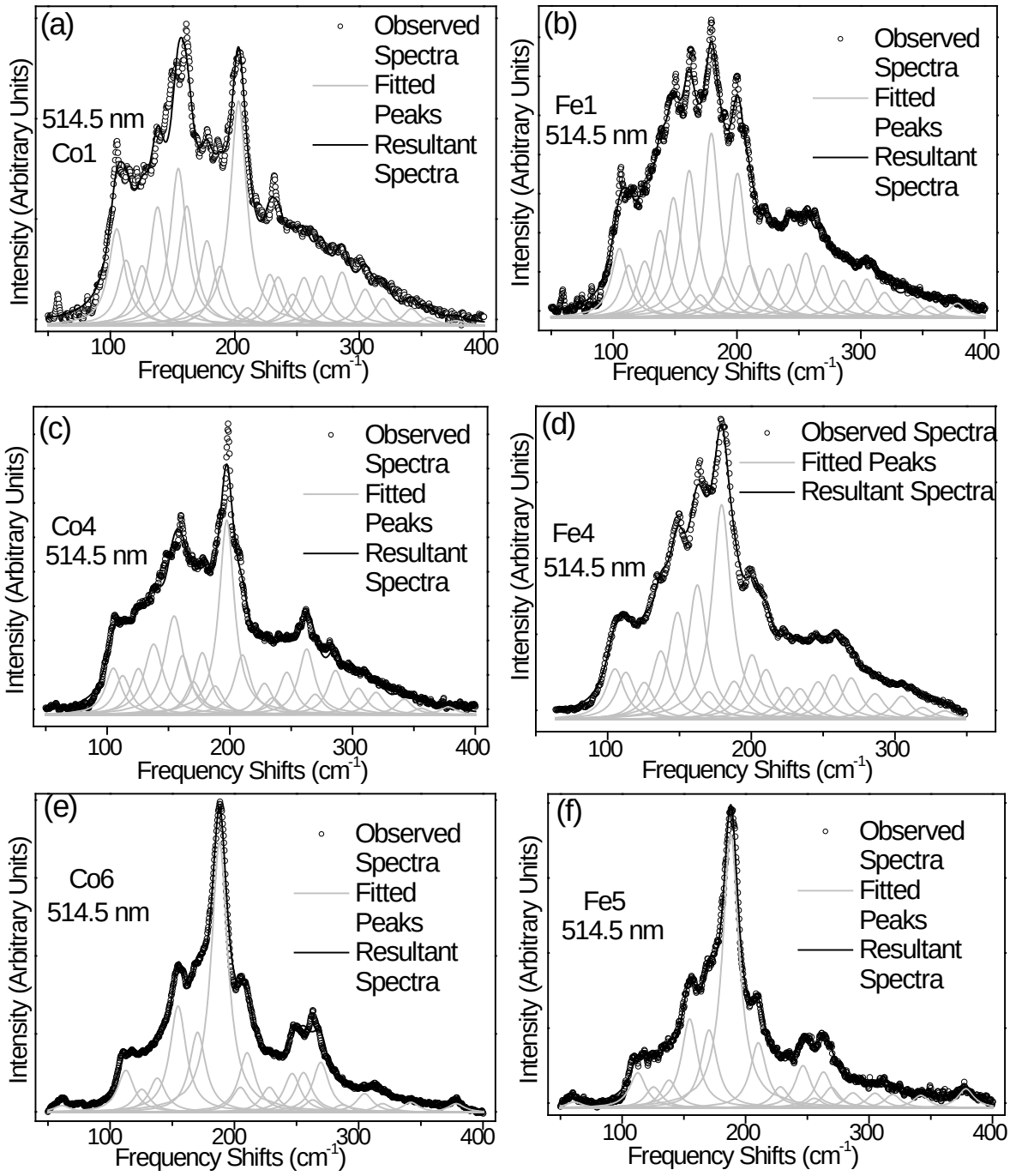

Figure 1: Deconvoluted RBM spectra of SWCNT samples recorded with 514.5 nm Ar^+ ion laser. The panels on the left ((a), (c) and (e)) are obtained from Co based catalysts while those on

the right ((b), (d) and (f)) from Fe based. The two spectra on the top ((a) and (b)) are grown with catalysts having the highest concentrations of Co or Fe, the two at the bottom ((e) and (f)) with the lowest concentrations while the ones at the middle ((c) and (d)) are grown with catalysts of intermediate concentrations.

Table 2: Details of the fitted RBM peaks and chiralities that most closely match these peaks for SWCNT samples prepared using low and high concentration catalysts. The spectra were obtained with 514.5 nm laser. For proper comparison between different samples the areas under the peaks were calculated after normalizing w.r.t. the most intense peak. Tubes obtained from the intermediate concentration catalysts are a subset of the tubes listed in the table.

Frequency (cm^{-1})	Co1	Co6	Fe1	Fe5	Diameter (nm)	Chiralities (n,m)	Area after normalization (cm^{-1}.nm)			
							Co1	Co6	Fe1	Fe5
61.31		✓		✓	4.560	39,27 38,28		0.025		0.022
105.11	✓		✓		2.460	24,11 31,0	0.430		0.375	
112.68	✓	✓	✓	✓	2.278	19,14 20,13 27,3	0.290	0.155	0.283	0.129
125.47	✓	✓	✓	✓	2.026	19,10 25,1	0.266	0.085	0.306	0.077
137.96	✓	✓	✓	✓	1.828	18,8	0.527	0.126	0.472	0.102
148.67			✓		1.687	16,8 17,7			0.650	
154.64	✓	✓		✓	1.617	18,4	0.699	0.394		0.326
161.45	✓		✓		1.545	15,7	0.532		0.797	
170.39	✓	✓	✓	✓	1.458	13,8	0.044	0.296	0.122	0.285
177.61	✓				1.396	17,1	0.377			
179.32			✓		1.381	12,8 11,9 15,4			1	
188.00	✓	✓	✓	✓	1.314	12,7 10,9, 14,4	0.262	1	0.221	1
200.47			✓		1.228	10,8			0.782	
204.79	✓	✓			1.201	12,5	1	0.092		
210.26	✓	✓	✓	✓	1.168	13,3	0.078	0.220	0.281	0.238
225.63			✓		1.085	12,3			0.264	
228.18	✓	✓		✓	1.072	13,1	0.227	0.092		0.077
234.85	✓				1.040	9,6	0.215			

241.58			✓		1.010	10,4 9,6			0.288	
246.47	✓	✓	✓	✓	0.989	10,4	0.139	0.143	0.026	0.155
255.64	✓	✓	✓	✓	0.952	12,0	0.212	0.147	0.349	0.035
263.04		✓		✓	0.924	8,5 12,0		0.046		0.131
269.50	✓	✓	✓	✓	0.901	8,5	0.220	0.185	0.281	0.075
286.88	✓	✓	✓	✓	0.845	10,1 9,3	0.237	0.027	0.201	0.055
304.74	✓	✓	✓	✓	0.793	10,0	0.161	0.069	0.209	0.054
319.19	✓	✓	✓	✓	0.756	6,5	0.119	0.032	0.136	0.049
341.92	✓	✓	✓	✓	0.704	7,3	0.074	0.037	0.103	0.046
355.82	✓		✓		0.676	8,1	0.035		0.061	
378.44	✓	✓	✓	✓	0.635	8,0	0.021	0.032	0.077	0.070

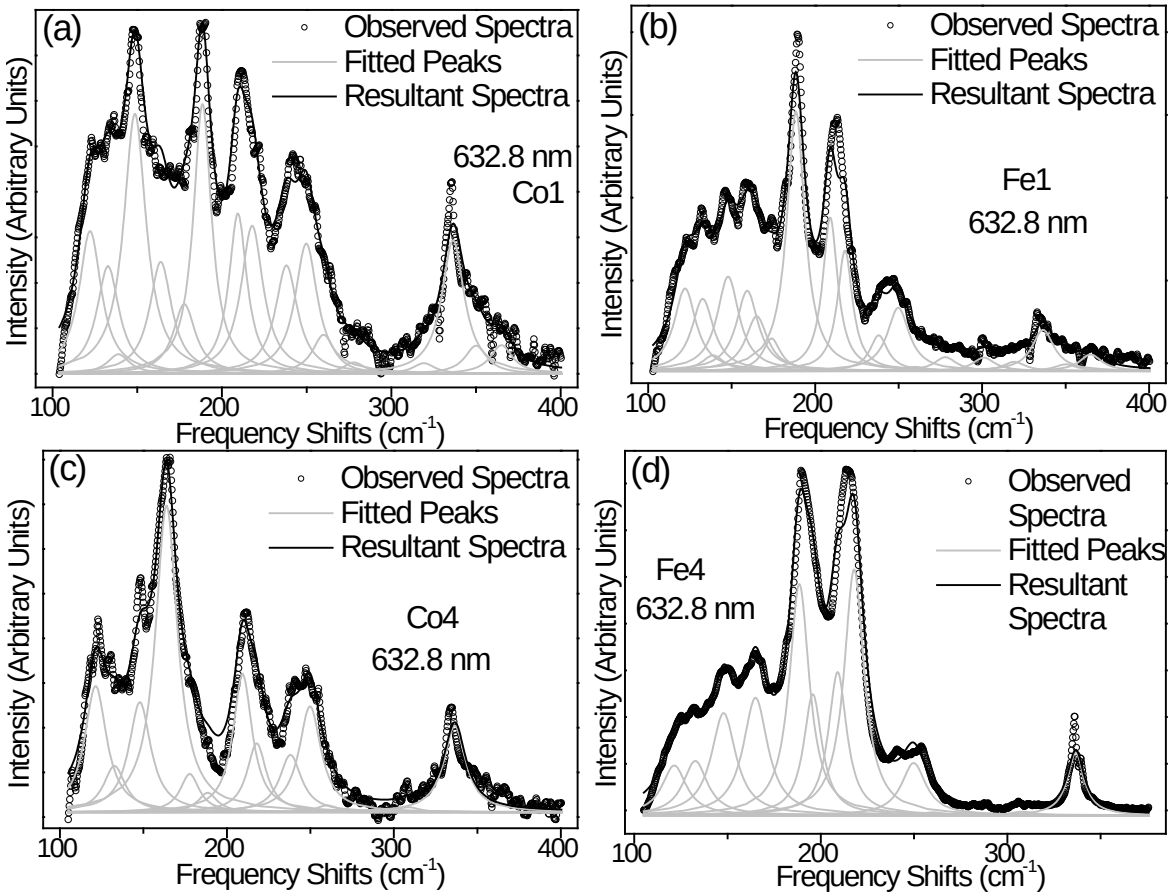

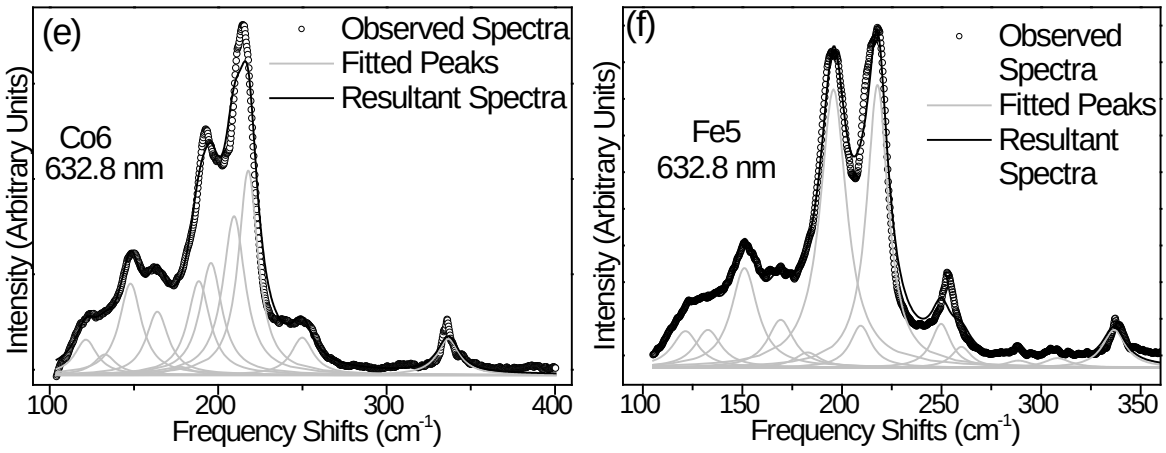

Figure 2: RBM spectra of SWCNTs obtained with 632.8 nm laser, fitted with Lorentzian peaks. Panels on the left ((a), (c) and (e)) are obtained from Co based catalysts while those on the right ((b), (d) and (f)) from Fe based. Top Panels ((a), (b)): SWCNTs grown with catalysts having the highest concentration of Co or Fe. Middle Panels ((c), (d)): intermediate concentrations. Bottom Panels ((e), (f)): lowest concentrations.

Table 3: Details of the fitted RBM peaks and chiralities that most closely match these peaks for SWCNT samples prepared using low and high concentration catalysts. The spectra were obtained with 632.8 nm laser. For proper comparison between different samples the areas under the peaks were calculated after normalizing w.r.t. the most intense peak. Tubes obtained from the intermediate concentration catalysts are a subset of the tubes listed in the table.

Frequency (cm^{-1})	Co1	Co6	Fe1	Fe5	Diameter (nm)	Chiralities (n,m)	Area after normalization (cm^{-1}.nm)			
							Co1	Co6	Fe1	Fe5
121.41	✓	✓	✓	✓	2.100	20,10 23,6 26,1	0.549	0.198	0.391	0.131
132.70	✓	✓	✓	✓	1.907	19,8 15,13	0.413	0.115	0.342	0.136
138.88	✓		✓		1.815	17,9	0.076		0.074	
147.89	✓	✓	✓		1.696	17,7	1	0.511	0.448	
151.01				✓	1.659	14,10 18,5				0.358
159.34			✓		1.566	16,6			0.380	

163.84	✓	✓			1.520	13,9 18,2	0.431	0.354		
165.00			✓		1.509	19,0 18,2			0.260	
169.20				✓	1.469	14,7				0.172
173.91			✓		1.427	18,0 17,2			0.125	
177.75	✓	✓			1.394	13,7	0.268	0.045		
182.77				✓	1.354	14,5				0.055
188.49	✓	✓	✓		1.310	16,1 11,8	0.843	0.525	1	
195.71		✓		✓	1.259	12,6		0.626		1
209.41	✓	✓	✓	✓	1.173	10,7	0.500	0.888	0.500	0.123
217.84	✓	✓	✓	✓	1.125	11,5	0.569	1	0.393	0.826
238.07	✓		✓		1.025	13,0	0.417		0.137	
249.88	✓	✓	✓	✓	0.975	9,5 8,6	0.501	0.209	0.300	0.118
260.00	✓		✓	✓	0.935	10,3	0.150		0.020	0.056
277.95	✓		✓		0.873	11,0	0.044		0.066	
288.51				✓	0.840	8,4				0.026
301.02			✓		0.804	9,2			0.064	
308.18				✓	0.784	8,3				0.034
319.17	✓		✓		0.756	9,1 6,5	0.041		0.043	
336.68	✓	✓	✓	✓	0.716	6,4	0.514	0.202	0.195	0.119
350.01	✓		✓		0.688	6,4	0.108		0.032	
365.03	✓		✓		0.659	7,2	0.110		0.078	

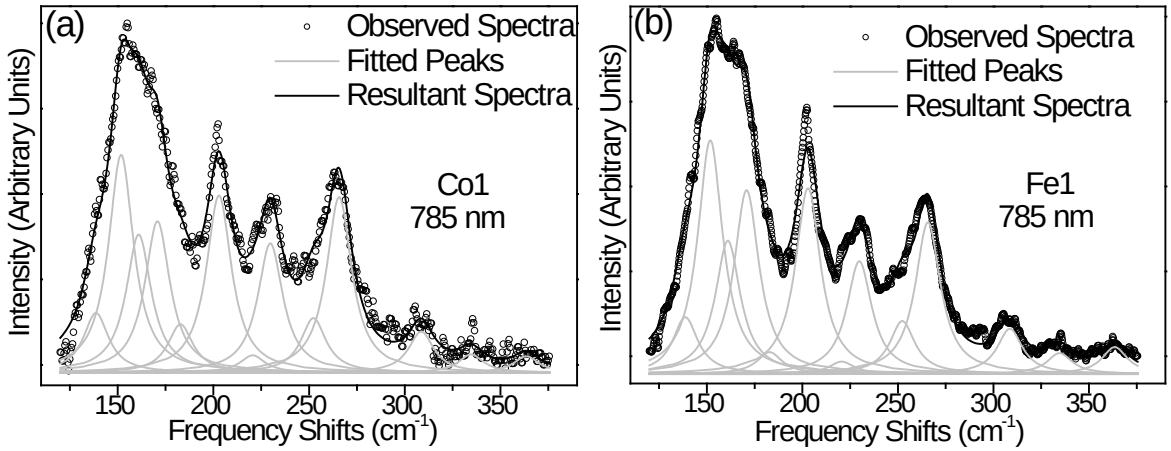

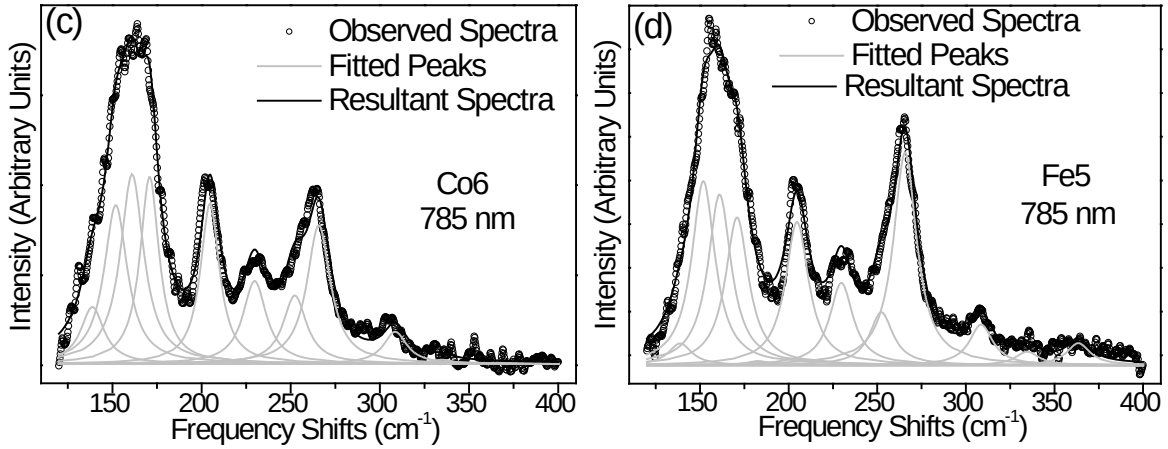

Figure 3: RBM spectra obtained with Raman spectrometer having 785 nm laser. Graphs on the left ((a), (c)) are obtained from Co based catalysts while those on the right ((b), (d)) from Fe based. Upper panels ((a), (b)): grown with catalysts having the highest concentration of Co or Fe. Lower panels ((c), (d)): lowest concentration. There is no appreciable difference between the spectra of the samples with Co or Fe or different concentrations of these active metals. Hence the spectra for the intermediate concentrations Co4 and Fe4 have not been shown as it does not provide any new information.

Table 4: Details of the fitted RBM peaks and chiralities that most closely match these peaks for SWCNT samples prepared using low and high concentration catalysts. The spectra were obtained with 785 nm laser. The areas under the peaks were calculated after normalizing w.r.t. the most intense peak.

Frequency (cm^{-1})	Co1	Co6	Fe1	Fe5	Diameter (nm)	Chiralities (n,m)	Area after normalization (cm^{-1}.nm)			
							Co1	Co6	Fe1	Fe5
138.70	✓	✓	✓	✓	1.818	20,5 18,8 16,10	0.274	0.300	0.243	0.102

151.80	✓	✓	✓	✓	1.650	12,12	1	0.837	1	0.865
161.00	✓	✓	✓	✓	1.549	19,1	0.634	1	0.570	0.801
170.80	✓	✓	✓	✓	1.455	16,4 12,9	0.695	0.801	0.786	0.694
182.81	✓	✓	✓	✓	1.354	14,5	0.222	0.013	0.093	0.020
204.71	✓	✓	✓	✓	1.212	12,5	0.813	0.686	0.795	0.673
220.54	✓		✓		1.111	14,0 10,6	0.080		0.053	
229.78	✓	✓	✓	✓	1.064	11,4	0.594	0.437	0.482	0.387
252.28	✓	✓	✓	✓	0.965	8,6 9,5	0.251	0.361	0.226	0.249
265.69	✓	✓	✓	✓	0.915	9,4	0.806	0.732	0.649	1
308.58	✓	✓	✓	✓	0.783	8,3	0.189	0.169	0.193	0.191
334.62	✓	✓	✓	✓	0.720	7,3	0.084	0.022	0.089	0.064
363.47	✓		✓	✓	0.662	7,2	0.076		0.115	0.104

The RBM spectra for Co6 and Fe5 are almost identical to each other for all the laser energies as shown in the lower panels of the figures 1, 2 and 3. They require almost the same set of Lorentz peaks for fitting. However as the concentration of the catalyst increases difference start appearing between the RBM spectra of Co and Fe samples. Surprisingly the RBM spectra obtained with 785 nm laser show no discernable difference between Co or Fe samples or with variation of catalyst concentration (figure 3).

As can be seen from the tables 2 - 4, a particular peak corresponding to a particular diameter may match closely with multiple tube chiralities that lie within the resonance window. There was always at least one tube within the resonance window. The tables also show the area under individual peaks obtained after normalizing w.r.t. the most intense peak in the spectrum under consideration. These values also represent the relative intensities of different peaks because the FWHMs of all the peaks have been kept the same. In the tables the chiralities of the intermediate concentrations Co4 and Fe4 have not been shown. A combination of the peaks present in samples with low and high concentrations of catalyst is sufficient to fit the spectrum of the samples with intermediate concentration. Hence the SWCNTs in Co4 or Fe4 are a subset of the

tubes shown in the tables. These have not been shown here to avoid overcrowding of data and because they do not provide any new information.

It is evident from the figures 1 and 2 that the RBM spectra become narrower as the concentration of Fe or Co decreases in the catalyst. This evolution is depicted more clearly in figure 4 by plotting the normalized RBM spectra for the three different catalyst compositions together in the same graph. A direct relation between peak intensity and the amount of the corresponding nanotube does not exist. However, since these spectra were recorded under the same experimental conditions with the same laser settings, one can assume that the decrease in relative intensity at a particular frequency would correlate directly with decrease in relative population of tubes with diameter corresponding to that frequency, while comparing between different samples.

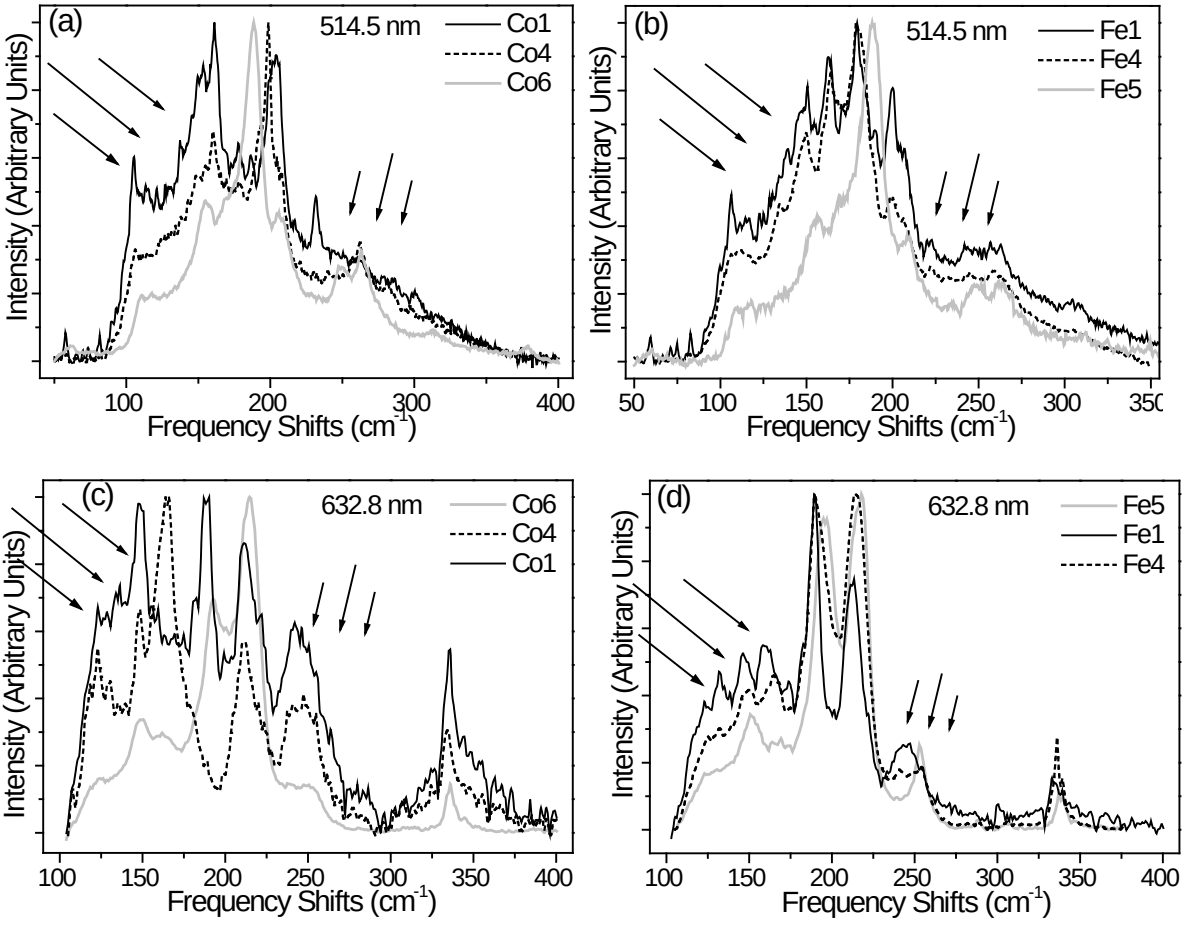

Figure 4: The narrowing of the RBM spectra as one goes from the high (Co1 and Fe1) to the low concentration (Co6 and Fe5) catalysts. Co4 and Fe4 have intermediate concentrations. The spectra were obtained with 514.5 nm (upper panels) and 632.8 nm (lower panels) laser excitations. Each spectrum has been normalized w.r.t. the most intense peak.

The most intense peak in the 514.5 nm RBM spectrum for Co6 is at 188 cm^{-1} (or 1.31 nm) and it alone contains 31% of the total area of the spectrum. The peaks in the range 188-154 cm^{-1}, i.e. 1.31-1.65 nm cover more than 50% of the total area. While in Co1 sample this range cover only 31% of the area and instead of a single dominant peak there are multiple high intensity peaks each containing around 10% area. Similarly in Fe5 the 188 cm^{-1} peak covers 34% area and the previously mentioned range accounts for 55% area, whereas in Fe1 the range only covers 35%. This lowering of the relative area of the peaks within these ranges with increase of catalyst concentration has been shown in figure 5 (a) and (b). The narrowing of diameter spread is more clearly visualized by plotting the positions of only the most intense peaks as has been done in figure 5 (c) and (d). However, with 785 nm laser no such narrowing of RBM spectrum was observed as is evident from figure 3. The reason behind this effect is not immediately clear from the experiments performed. Different synthesis techniques like laser ablation, CVD with supported catalysts, CVD with thin film catalysts or plasma assisted techniques generally give rise to different chiralities. In other words different chiralities behave differently under different growth conditions. The chiralities that resonate with 785 nm laser are mostly different from those that resonate with 514.5 and 632.8 nm lasers. Those chiralities that are common either have very low intensities in one of the spectra or have other possible chiral matches for the same peak. It is possible that the chiralities of the 785 nm spectra are not very sensitive to catalyst concentrations. Further studies are needed to understand this process.

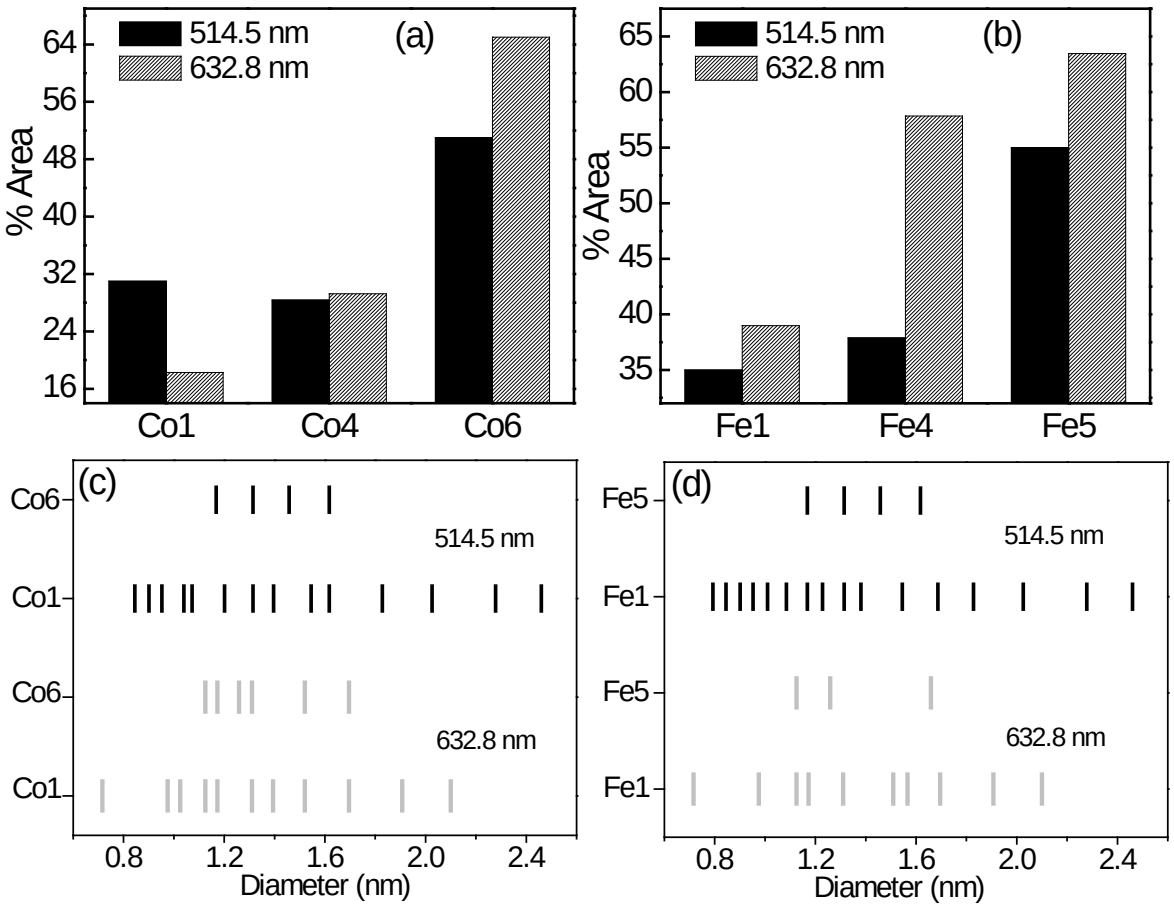

Figure 5: Majority of the tubes in the low concentration catalysts Co6 and Fe5 are confined within small diameter ranges. This range as observed in the 514.5 nm laser spectra is 1.31-1.65 nm and in the 632.8 nm laser spectra it is 1.13-1.35 nm. (a) and (b) Percentages of the total area under RBM that fall within these ranges for SWCNTs grown with different catalysts. These percentages are clearly higher in both Co6 and Fe5 as compared to Co1 and Fe1. (c) and (d) Positions of the most intense RBM peaks for SWCNTs grown with different Fe and Co catalysts. For the 514.5 nm RBM spectra peaks with relative intensity of 0.2 or above have been plotted and for the 632.8 nm spectra peaks with relative intensity $\geq$ 0.25 have been considered. The narrowing of the diameter spread for Co6 and Fe5 is very clearly observable.

Thus there was partial success in restricting the diameter spread of the SWCNTs by lowering the concentration of the Co or Fe catalyst in MgO matrix. This is presumably due to formation of smaller catalyst nanoparticles during the CVD process. As stated above, the diameter ranges 1.31-1.65 nm and 1.13-1.31 nm command the major share of the area under the RBM curves of

Co6 and Fe5 samples, as observed with 514.5 nm and 632.8 nm lasers, respectively. In the 785 nm spectra of Co6 the diameter range 1.46-1.65 nm cover 50% area and the tube of diameter 1.20 nm alone account for 12% area. Similarly in the 785 nm spectra of Fe5 the same diameter range accounts for 46% area and the 1.20 nm tube covers 13% area. Thus, on the basis of the resonance Raman scattering it can be concluded that the major fraction of the SWCNTs synthesized using low concentration catalyst have diameters lying between 1.13 and 1.65 nm.

It is worth mentioning that there was no observed preference in terms of chirality or chiral angle in the tubes grown using all the different catalyst compositions. This can be seen from figure 6. It also means that there will be both semiconducting and metallic tubes present in the samples without much control over their relative proportions. However, majority of the tubes synthesized by this technique seem to lie within an angular spread of 25.5^0, between the chiral angles 2.5^0 and 28^0 as sown in figure 6. The relative intensities of the different RBM peaks in Fe5 and Co6 samples were taken into account while arriving at this conclusion. A more detailed diagram showing the chiral distribution of the tubes obtained from each of the different catalysts is shown in the supporting information (figure S5).

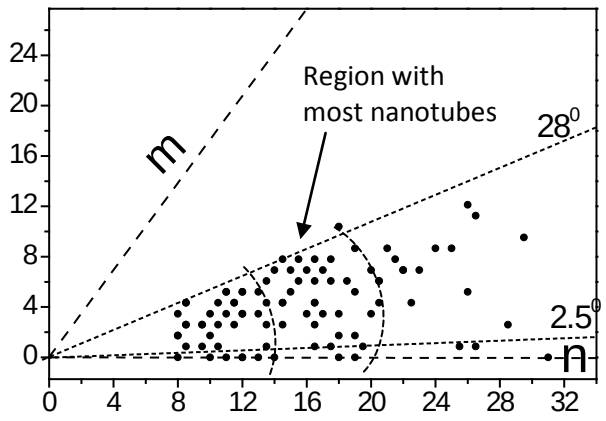

Figure 6: Chiral distribution of the synthesized SWCNTs. The region containing the majority of the SWCNTs synthesized with low concentration Fe5 and Co6 catalysts have been demarcated in the figure. The angular range between 2.5^0 and 28^0 contain most of the tubes. The directions of these chiral angles and the primitive vectors of the graphene lattice (labelled as m and n) are

shown as dashed lines. The arcs represent the diameter range, 1.13 to 1.65 nm, wherein most of the Fe5 and Co6 SWCNTs lie.

The G bands (~ 1580 cm^{-1}) in the Raman spectra of the SWCNTs did not provide any useful information. In SWCNTs the G band has multiple peaks with G^- and G^+ being the most prominent ones. We found that three peaks were sufficient to fit the G bands (please see figure S4 in supporting information). The G^- peak depends on the diameter as well as on the conducting nature of the tubes. However, unlike the RBMs, the diameter dependence is very mild [29,33] and in the presence of several resonating tubes with similar diameters, all one can observe is a broad G^- peak.

Some typical TEM images of the samples have been shown in figure 7. We found it rather difficult to obtain high magnification images of SWCNTs, even in a high resolution TEM. The tubes are generally entangled in bundles. Attempts to separate them by prolonged ultra-sonication damaged the tubes. Exposure to the electron beam was also found to damage the walls of the tubes. Hence the microscopic data was not sufficient enough to analyze the relative abundance of the nanotubes of each and every chirality or diameter. Nonetheless, the average diameters of the tubes in different samples were estimated from the limited microscopic data. The mean diameters for both the low concentration samples, Co6 and Fe5, were found to be 1.2 ± 0.3 nm. For the high concentration samples, Co1 and Fe1, the mean diameters were 1.4 ± 0.4 nm and 1.4 ± 0.3 nm, respectively. Although microscopic observation is a more straight forward method for diameter determination the technical difficulties associated with it make the spectroscopic techniques more attractive. Microscopy has not been used in previous studies dealing with selective synthesis [2,4-6,8] or separation [10-13] of SWCNTs in bulk amounts.

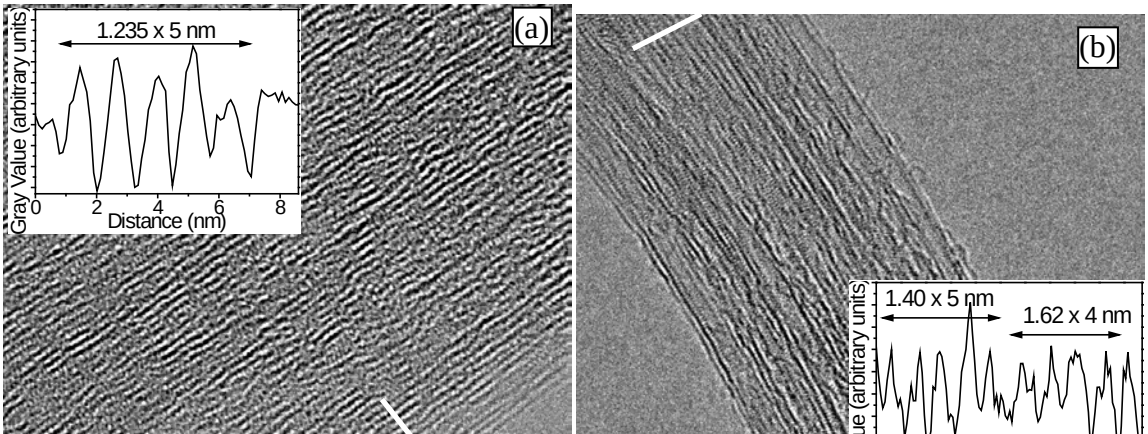

Figure 7: High magnification TEM image of SWCNT bundles obtained from the samples (a) Co6 (scale bar is 10 nm); (b) Co1 (scale bar is 20 nm). The gray scale profiles of the image along the white bars are shown in the insets. The diameters of the tubes were estimated using such profiles. The values of the diameters shown here correspond only to these particular images.

The structural integrity of the SWCNTs was estimated using the D band (~ 1350 cm^{-1}) of the Raman spectra. The ratio of the intensities of the D band (I_D) to the G band (I_G) provides a measure of the defects in the sp^2 structure of the nanotube walls [29,33]. Mean values of the I_D/I_G ratios have been shown in the table 5. Best ratios were obtained from the Fe5 and Co6 SWCNT samples. The amount of SWCNTs and other carbonaceous material that could be grown by a catalyst depended upon its composition. As expected, a catalyst with higher concentration of Fe or Co in the MgO matrix produced higher amounts of carbonaceous substances per unit mass of the catalyst. Table 5 shows the yields from different catalysts. The yield was estimated by measuring the change in weight when the nanotubes + catalyst mixture is treated with 11M HNO_3 solution. The acid dissolves MgO and the metal catalyst leaving behind SWCNTs and other carbon impurities. This procedure is described in detail in reference [28]. Interestingly, the SWCNT samples with the best I_D/I_G ratios have the lowest yields of about 1-2 weight percent. It must be noted that the low values of yields are due to the fact that these have been calculated w.r.t. the total weight of the catalyst and the support material. If one considers only the weight of the active catalysts, i.e. Co or Fe for the purpose of calculating the yields then the values are much higher. For example the yield of carbon w.r.t. Co in Co6 392% and w.r.t Fe in Fe5 it is 423%.

Table 5: I_D/I_G ratios of the SWCNTs and the yield of carbonaceous materials synthesized using the different catalyst compositions.

SWCNT sample	I_D/I_G Ratio	Yield (%)
Co1	0.20	44.2
Fe1	0.18	20.6
Co4	0.16	9.1
Fe4	0.13	6.1
Co6	0.09	1.3
Fe5	0.10	2.1

Another important factor that was considered while adjudicating the quality of the samples is the amount of carbon based impurities present in the samples, other than the SWCNTs. These include amorphous carbon, onion like multilayer graphitic shells with or without a catalyst nanoparticle enclosed in them, multi-wall nanotubes mostly with deformed bamboo like shape, etc. TEM images of theses impurities have been shown in the supporting information (figure S6). These are extremely difficult to remove and a major hurdle in any application of the nanotubes. Hence, although Co1 and Fe1 have very high yields with tolerable I_D/I_G ratios, the high levels of carbon impurities make their use in several applications impractical. This impurities result due to the formation of bigger catalyst nanoparticles when the concentration is high. Tang, et al had also observed that increase in the amount of Co in the catalyst can lead to an increase in relative population of multi-walled carbon nanotubes [20].

4. Conclusion

We were able to reduce the diameter spread of SWCNTs synthesized using ordinary CVD process, by reducing the concentration of the active bi-metal catalyst in MgO support. The

catalyst was prepared by combustion technique. Structural characterization of the SWCNTs was carried out using the Raman spectra obtained with three different laser wavelengths; 514.5, 632.8 and 785 nm. The most probable diameters and chiralities of the nanotubes were identified by fitting the RBM spectra and using a Kataura plot. With low concentration catalysts (Co:Mo:MgO = 1:0.5:300 and Fe:Mo:MgO = 1:0.5:200) the diameter spread could be restricted to a range of 1.13 to 1.65 nm. Lowering the catalyst concentration was also instrumental in decreasing the I_D/I_G ratio and eliminating carbonaceous impurities. The main advantage of our technique lies in its simplicity. The preliminary results are encouraging and further studies can lead to better control on chirality.

Author Contributions

S.R. carried out most of the work. R.B. helped with many of the experiments. D.S.M. helped with the analysis. N.S., S.S.R. and J.A.M. helped with the Raman scattering measurements using 632.8 and 785 nm lasers. All the authors have contributed towards the successful completion of the project and the manuscript.

Acknowledgements

Authors acknowledge the Centre for Research in Nanotechnology & Science (CRNTS), IIT Bombay, for facilitating most of the measurements done in this study. S.R. would like to thank the British Council (United Kingdom-India Education and Research Initiative –UKIERI) for funding his work at the University of Ulster

References

[1] M. C. Hersam, Progress towards monodisperse single-walled carbon nanotubes, Nat Nano 3 (2008) 387-394.

[2] W.-H. Chiang, R. Mohan Sankaran, Linking catalyst composition to chirality distributions of as-grown single-walled carbon nanotubes by tuning NixFe1-x nanoparticles, Nat. Mater. 8 (2009) 882-886.

[3] Y. Li, W. Kim, Y. Zhang, M. Rolandi, D. Wang, H. Dai, Growth of Single-Walled Carbon Nanotubes from Discrete Catalytic Nanoparticles of Various Sizes, J. Phys. Chem. B 105 (2001) 11424-11431.

[4] W.-H. Chiang, M. Sakr, X. P. A. Gao, R. M. Sankaran, Nanoengineering NixFe1−x Catalysts for Gas-Phase, Selective Synthesis of Semiconducting Single-Walled Carbon Nanotubes, ACS Nano 3 (2009) 4023-4032.

[5] L. Ding, A. Tselev, J. Wang, D. Yuan, H. Chu, T. P. McNicholas, Y. Li, J. Liu, Selective Growth of Well-Aligned Semiconducting Single-Walled Carbon Nanotubes, Nano Lett. 9 (2009) 800-805.

[6] L. Qu, F. Du, L. Dai, Preferential Syntheses of Semiconducting Vertically Aligned Single-Walled Carbon Nanotubes for Direct Use in FETs, Nano Lett. 8 (2008) 2682-2687.

[7] Y. Zhao, H. Nakano, H. Murakami, T. Sugai, H. Shinohara, Y. Saito, Controllable growth and characterization of isolated single-walled carbon nanotubes catalyzed by Co particles, Appl. Phys. A 85 (2006) 103-107.

[8] M. Fouquet, B. C. Bayer, S. Esconjauregui, C. Thomsen, S. Hofmann, J. Robertson, Effect of Catalyst Pretreatment on Chirality-Selective Growth of Single-Walled Carbon Nanotubes, J. Phys. Chem. C 118 (2014) 5773-5781.

[9] Y. Su, Z. Yang, H. Wei, E. S.-W. Kong, Y. Zhang, Synthesis of single-walled carbon nanotubes with selective diameter distributions using DC arc discharge under CO mixed atmosphere, Appl. Surf. Sci. 257 (2011) 3123-3127.

[10] M. S. Arnold, A. A. Green, J. F. Hulvat, S. I. Stupp, M. C. Hersam, Sorting carbon nanotubes by electronic structure using density differentiation, Nat Nano 1 (2006) 60-65.

[11] A. Nish, J.-Y. Hwang, J. Doig, R. J. Nicholas, Highly selective dispersion of single-walled carbon nanotubes using aromatic polymers, Nat Nano 2 (2007) 640-646.

[12] P. G. Collins, M. S. Arnold, P. Avouris, Engineering Carbon Nanotubes and Nanotube Circuits Using Electrical Breakdown, Science 292 (2001) 706-709.

[13] G. Zhang, P. Qi, X. Wang, Y. Lu, X. Li, R. Tu, S. Bangsaruntip, D. Mann, L. Zhang, H. Dai, Selective Etching of Metallic Carbon Nanotubes by Gas-Phase Reaction, Science 314 (2006) 974-977.

[14] J. W. Song, H. W. Seo, J. K. Park, J. E. Kim, D. G. Choi, C. S. Han, Selective removal of metallic SWNTs using microwave radiation, Curr. Appl Phys. 8 (2008) 725-728.

[15] N. Li, G. Lee, J. W. Yang, H. Kim, M. S. Yeom, R. H. Scheicher, J. S. Kim, K. S. Kim, Noncovalent Functionalization with Alkali Metal to Separate Semiconducting from Metallic Carbon Nanotubes: A Theoretical Study, J. Phys. Chem. C 117 (2013) 4309-4313.

[16] M. Terrones, Science and Technology of the Twenty-First Century: Synthesis, Properties, and Applications of Carbon Nanotubes, Annu. Rev. Mater. Res. 33 (2003) 419-501.

[17] E. Flahaut, A. Peigney, C. Laurent, A. Rousset, Synthesis of single-walled carbon nanotube-Co-MgO composite powders and extraction of the nanotubes, J. Mater. Chem. 10 (2000) 249-252.

[18] L. Qingwen, Y. Hao, C. Yan, Z. Jin, L. Zhongfan, A scalable CVD synthesis of high-purity single-walled carbon nanotubes with porous MgO as support material, J. Mater. Chem. 12 (2002) 1179-1183.

[19] E. Flahaut, R. Bacsa, A. Peigney, C. Laurent, Gram-scale CCVD synthesis of double-walled carbon nanotubes, Chem. Commun. (2003) 1442-1443.

[20] S. Tang, Z. Zhong, Z. Xiong, L. Sun, L. Liu, J. Lin, Z. X. Shen, K. L. Tan, Controlled growth of single-walled carbon nanotubes by catalytic decomposition of CH4 over Mo/Co/MgO catalysts, Chem. Phys. Lett. 350 (2001) 19-26.

[21] B. C. Liu, S. C. Lyu, S. I. Jung, H. K. Kang, C. W. Yang, J. W. Park, C. Y. Park, C. J. Lee, Single-walled carbon nanotubes produced by catalytic chemical vapor deposition of acetylene over Fe–Mo/MgO catalyst, Chem. Phys. Lett. 383 (2004) 104-108.

[22] Y. Zhang, Q. Yu, X. Wang, Y. Tian, A new understanding of carbon nanotube growth: Activation and deactivation of a catalyst, Appl. Surf. Sci. 298 (2014) 221-224.

[23] X. Fu, X. Cui, X. Wei, J. Ma, Investigation of low and mild temperature for synthesis of high quality carbon nanotubes by chemical vapor deposition, Appl. Surf. Sci. 292 (2014) 645-649.

[24] A.-N. A. El-Hendawy, R. J. Andrews, A. J. Alexander, Impact of Mo and Ce on growth of single-walled carbon nanotubes by chemical vapour deposition using MgO-supported Fe catalysts, Appl. Surf. Sci. 255 (2009) 7446-7450.

[25] Y. H. Hu, E. Ruckenstein, Binary MgO-based solid solution catalysts for methane conversion to syngas, Catalysis Reviews 44 (2002) 423-453.

[26] S. Roy, R. Bajpai, N. Soin, P. Bajpai, K. S. Hazra, N. Kulshrestha, S. S. Roy, J. A. McLaughlin, D. S. Misra, Enhanced Field Emission and Improved Supercapacitor Obtained from Plasma-Modified Bucky Paper, Small 7 (2011) 688-693.

[27] S. Roy, R. Bajpai, A. K. Jena, P. Kumar, N. kulshrestha, D. S. Misra, Plasma modified flexible bucky paper as an efficient counter electrode in dye sensitized solar cells, Energy Environ. Sci. 5 (2012) 7001-7006.

[28] S. Roy, V. Jain, R. Bajpai, P. Ghosh, A. S. Pente, B. P. Singh, D. S. Misra, Formation of Carbon Nanotube Bucky Paper and Feasibility Study for Filtration at the Nano and Molecular Scale, J. Phys. Chem. C 116 (2012) 19025-19031.

[29] M. S. Dresselhaus, G. Dresselhaus, R. Saito, A. Jorio, Raman spectroscopy of carbon nanotubes, Phys. Rep. 409 (2005) 47-99.

[30] M. S. Strano, S. K. Doorn, E. H. Haroz, C. Kittrell, R. H. Hauge, R. E. Smalley, Assignment of (n, m) Raman and Optical Features of Metallic Single-Walled Carbon Nanotubes, Nano Lett. 3 (2003) 1091-1096.

[31] S. M. Bachilo, M. S. Strano, C. Kittrell, R. H. Hauge, R. E. Smalley, R. B. Weisman, Structure-Assigned Optical Spectra of Single-Walled Carbon Nanotubes, Science 298 (2002) 2361-2366.

[32] Z. Yu, L. Brus, Rayleigh and Raman Scattering from Individual Carbon Nanotube Bundles, J. Phys. Chem. B 105 (2001) 1123-1134.

[33] A. Jorio, M. A. Pimenta, A. G. S. Filho, R. Saito, G. Dresselhaus, M. S. Dresselhaus, Characterizing carbon nanotube samples with resonance Raman scattering, New J. Phys. 5 (2003) 139.131-139.117.

[34] M. S. Dresselhaus, G. Dresselhaus, A. Jorio, A. G. Souza Filho, R. Saito, Raman spectroscopy on isolated single wall carbon nanotubes, Carbon 40 (2002) 2043-2061.

[35] A. Jorio, R. Saito, J. H. Hafner, C. M. Lieber, M. Hunter, T. McClure, G. Dresselhaus, M. S. Dresselhaus, Structural (n,m) Determination of Isolated Single-Wall Carbon Nanotubes by Resonant Raman Scattering, Phys. Rev. Lett. 86 (2001) 1118-1121.

[36] P. T. Araujo, P. B. C. Pesce, M. S. Dresselhaus, K. Sato, R. Saito, A. Jorio, Resonance Raman spectroscopy of the radial breathing modes in carbon nanotubes, Physica E 42 (2010) 1251-1261.

[37] H. Kataura, Y. Kumazawa, Y. Maniwa, I. Umezu, S. Suzuki, Y. Ohtsuka, Y. Achiba, Optical properties of single-wall carbon nanotubes, Synth. Met. 103 (1999) 2555-2558.

[38] R. Saito, G. Dresselhaus, M. S. Dresselhaus, Trigonal warping effect of carbon nanotubes, Phys. Rev. B 61 (2000) 2981-2990.

[39] J. Han, Structures and Properties of Carbon Nanotubes, in: M. Meyyappan (Eds.), Carbon nanotubes: science and applications, CRC press, Boca Raton, 2004.

[40] S. Reich, C. Thomsen, J. Maultzsch, Carbon nanotubes: basic concepts and physical properties, John Wiley & Sons, Weinheim, 2008.

[41] M. S. Dresselhaus, A. Jorio, R. Saito, Characterizing Graphene, Graphite, and Carbon Nanotubes by Raman Spectroscopy, Annu. Rev. Condens. Matter Phys. 1 (2010) 89-108.

[42] A. Jorio, C. Fantini, M. A. Pimenta, R. B. Capaz, G. G. Samsonidze, G. Dresselhaus, M. S. Dresselhaus, J. Jiang, N. Kobayashi, A. Grüneis, R. Saito, Resonance Raman spectroscopy (n,m)-dependent effects in small-diameter single-wall carbon nanotubes, Phys. Rev. B 71 (2005) 075401.